Final Report

Inverse Problem Approaches for Bridge Structural Health Monitoring Using Displacement Data

Claudia Marin-Artieda, Ph.D., P.E.

Howard University

Phone: 202-806-8568; Email: cmarin@howard.edu

Date

August 2026

Prepared for the Safety and Mobility Advancement Regional Transportation and Economics Research Center, Morgan State University, CBEIS 327, 1700 E. Coldspring Lane, Baltimore, MD 21251

ACKNOWLEDGMENT

This research was supported by the Safety and Mobility Advancement Regional Transportation and Economics Research Center at Morgan State University and the University Transportation Center(s) Program of the U.S. Department of Transportation.

Disclaimer

The contents of this report reflect the views of the authors, who is responsible for the facts and the accuracy of the information presented herein. This document is disseminated in the interest of information exchange. The report is funded, partially or entirely, under grant number 69A3552348303 from the U.S. Department of Transportation's University Transportation Centers Program. The U.S. Government assumes no liability for the contents or use thereof.

1. Report No. SM19	2. Government Accession No.	3. Recipient's Catalog No.
4. Title and Subtitle Inverse Problem Approaches for Bridge Structural Health Monitoring Using Displacement Data		**5. Report Date** May 2025 to May 2026
		6. Performing Organization Code
7. Author(s) Claudia Marin-Artieda, ORCID 0000-0002-4361-7671		**8. Performing Organization Report No.**
9. Performing Organization Name and Address Howard University Department of Civil and Environmental Engineering 2300 6th Street NW, Washington, DC 20059		**10. Work Unit No.**
		11. Contract or Grant No. 69A3552348303
12. Sponsoring Agency Name and Address US Department of Transportation Office of the Secretary-Research UTC Program, RDT-30 1200 New Jersey Ave., SE Washington, DC 20590		**13. Type of Report and Period Covered** Final, May 2025 to May 2026
		14. Sponsoring Agency Code

15. Supplementary Notes

16. Abstract

This project developed and validated an inverse problem framework for truss bridges that uses displacement as the primary diagnostic input. Displacement histories are extracted from single-camera video by optical flow tracking, modal parameters are identified by output-only methods with bootstrap uncertainty quantification, and element-level damage indices are formed from the resulting mode shapes. The framework was demonstrated through three progressive laboratory studies: global stiffness identification from a single tracked joint on a spring-mounted Warren truss; element-level localization on a fourteen-bay benchmark truss using finite-element response with synthetic noise; and element-level localization on the same benchmark truss using video-derived displacement. Both video cases identified the damaged member at rank one within the correct bay. Localization is reliable at stiffness reductions of thirty percent and above. At lower severities, identification remains confined to the correct bay although the individual member is not consistently ranked first. Severity is reported as a normalized indicator score rather than a calibrated stiffness loss, and calibration of that mapping is identified as the principal remaining step.

17. Key Words:	**18. Distribution Statement**
Structural health monitoring; bridge inspection; computer vision; displacement measurement; inverse problems; modal strain energy; damage localization; transportation asset management	No restrictions. This document is available to the public

19. Security Classif. (of this report) :	20. Security Classif. (of this page)	21. No. of Pages	22. Price
Unclassified	Unclassified		

Table of Contents

Abstract ii
Introduction 1
Problem and Motivation 1
Objectives 1
Report Organization 1
Literature Review 2
Inverse Problems in Structural Dynamics 2
Solution Families and Their Assumptions 2
The Measured Displacement Histories as a Choice 3
Vision-Based Displacement Measurement 4
Method Selection 4
Data Description 5
Small-Scale Warren Truss Specimen 5
Fourteen-Bay Benchmark Truss Specimen 5
Damage Cases 6
Measurement Configuration 6
Methodology 7
Displacement Extraction from Video 7
Output-Only Modal Identification 8
Uncertainty Quantification 8
Elemental Modal Strain Energy 9
Normalization and Interpretation of the Indicator 10
Global Identification for the Single-Degree-of-Freedom Case 11
Results 11
Global Damage Identification from a Single Tracked Joint 11
Element-Level Localization from Simulated Response 13
Severity Calibration and Family-Specific Behavior 13
Element-Level Localization from Video-Derived Displacement 14
Interpretation of the Contrast Between Cases 15
Conclusion 16
Findings 16
Limitations 16
Future Work 17
References 17

Abstract

Transportation agencies manage large inventories of aging assets under constrained budgets. Condition assessment of bridges, pedestrian bridges, cantilevered signal structures, and similar installations remains predominantly reactive, relying on visual inspection that is labor-intensive, subjective, and unable to detect deterioration before it becomes visible. Instrumented alternatives based on contact sensor networks provide quantitative information but require installation, cabling, and maintenance that limit the number of assets that can practically be monitored.

This project developed and validated an inverse problem framework for bridge structural health monitoring, demonstrated here on truss specimens, that uses displacement as the primary diagnostic input. Displacement time histories are extracted from single-camera video by optical flow tracking. Modal parameters are then identified by output-only methods, with bootstrap resampling used to quantify the uncertainty of the identified quantities, and element-level damage indices are formed from the resulting mode shapes.

The framework was demonstrated through three progressive laboratory studies. A spring-mounted Warren truss established that global stiffness change can be identified from a single tracked joint. A fourteen-bay benchmark truss, analyzed first with finite-element response contaminated by synthetic noise, established element-level localization under controlled conditions. The same benchmark truss was then analyzed using video-derived displacement, and in both damage cases examined, the framework identified the damaged member at rank one within the correct bay.

Localization is reliable at stiffness reductions of thirty percent and above. At lower severities, indicator activity remains confined to the correct bay although the individual member is not consistently ranked first, which suggests the bay as the appropriate reporting unit in that range rather than the member. Severity is reported as a normalized indicator score rather than a calibrated stiffness loss, and calibration of that mapping on an element-family basis is identified as the principal remaining step before field deployment.

Introduction

Problem and Motivation

Assessment of transportation infrastructure assets remains predominantly reactive. In most instances, inspection occurs only after visible deterioration or outright failure and relies almost exclusively on visual examination that is labor intensive, subjective, and expensive. Critical assets therefore remain vulnerable to undetected degradation, and maintenance resources are allocated on incomplete information. As the national inventory continues to age under constrained budgets, there is a clear need for condition assessment methods that are automated, scalable across many assets, and inexpensive enough to apply routinely.

Instrumented monitoring offers a quantitative alternative, but conventional contact-sensor networks impose costs that scale with the number of measurement points. Installation, cabling, power, and long-term maintenance limit the spatial density achievable and, in practice, the number of structures that can be monitored. The intent of this work is not to displace contact instrumentation, however. A small number of accelerometers remain an affordable and effective means of establishing reference measurements. The objective is rather to extend spatial coverage beyond what a limited sensor set can provide, using measurements that require no attachment to the structure.

Computer vision offers such a route. Optical flow methods applied to standard video can recover sub-pixel displacements at many points simultaneously, without physical contact and without interrupting the asset's operation. The camera requirement is that it provides adequate frame rate and spatial resolution, together with the associated tracking software. Given those conditions, video cameras can supply a spatially distributed displacement field of a kind that would otherwise require a dense and costly sensor array.

Objectives

The project set out to establish whether displacement measured in this way can support quantitative inverse identification of structural conditions. Four objectives follow from that aim. The first is to review dynamic inverse problems in structural engineering and identify the methods and assumptions appropriate to displacement data. The second is to formulate a methodology that infers structural parameters, in particular stiffness reduction and its location, directly from displacement measurements. The third is to test that methodology numerically under controlled conditions where the damage state is known exactly. The fourth is to validate it against measured data from a physical specimen under prescribed damage.

Report Organization

The report is organized as follows. The literature review situates the work within inverse problem theory and identifies the solution family adopted here. The data description presents the specimens, the damage cases, and the measurement configurations. The methodology sets out the processing methods from video to damage index. The results present three progressive studies, beginning with global identification from a single tracked point and concluding with element-level localization from video-derived displacement on the benchmark truss. The conclusion summarizes findings, states limitations, and defines the work required to move the framework toward field application.

Literature Review

Inverse Problems in Structural Dynamics

Structural analysis is conventionally practiced as a forward problem. Given the external forces, geometry, member sizes, and restraint conditions, the response of the structure is computed. Gallet et al. (2022), in a review spanning design, assessment, non-destructive evaluation, and smart structures, observe that this forward formulation is what entry-level structural engineering instruction establishes, and that a substantial portion of contemporary assessment practice in fact requires its inversion: the response is measured, and the properties that produced it are sought.

Condition assessment belongs to this inverse category. The measured quantity is a structural response, and the unknown is a property of the structure itself, most often a stiffness distribution. Two consequences follow and shape everything downstream. The first is that the number of unknowns is set by the structure, so a truss with fifty members presents fifty candidate parameters regardless of how many sensors are deployed. The second is that the mapping from properties to response is not generally invertible in a stable sense, because different property distributions can produce responses that differ by less than the measurement error. The practical difficulty in structural damage identification is therefore rarely the inversion algorithm itself. As Friswell (2007) observes, damage is local in nature, so although its effect may be described by few parameters, not knowing its location requires that many candidate parameters be carried, and the resulting imbalance against the available measurements leads to ill-conditioning. This observation motivates the emphasis placed in the present work on obtaining many spatially distributed measurement points at low cost.

Solution Families and Their Assumptions

Three broad families of solutions are available, and each carries requirements that determine where it can be applied.

Model updating adjusts the parameters of a finite-element model until its computed response matches measurement. Hester et al. (2019) apply this approach to bridges with particular attention to support conditions. The method is powerful where a validated model exists, but that requirement is substantial: it presumes a model whose form is correct and whose remaining uncertainty is confined to the parameters being updated. Where the number of candidate parameters approaches the number of independent measurements, the updated solution is not unique, and several parameter sets will reproduce the measured response equally well.

Modal indicator methods form the second family. Rather than updating a model, they compute a scalar quantity for each element from measured modal properties and compare its value between a reference state and a test state. Cawley and Adams (1979) established that ratios of natural frequency change carry information about damage location. Pandey et al. (1991) showed that mode shape curvature is more sensitive to local stiffness loss than the mode shape itself. Shi et al. (2000) introduced the modal strain energy change approach, in which each element's share of the total modal strain energy is compared between states, with a reduction in that share indicating local softening. Catbas et al. (2006) developed modal flexibility indices and demonstrated their tolerance to mode truncation on large structures. The defining requirement of this family is modest: two measurements of the same structure, and one taken as reference. No knowledge of the excitation is needed, which suits structures under ambient loading.

Data-driven methods form the third family. Bao et al. (2025) reviewed the growth of machine learning in structural health diagnosis and noted that the essence of monitoring lies in diagnosing structural condition by analyzing measured data, a framing that admits methods making no explicit mechanical assumption. The general limitation of data-driven approaches for civil structures is the requirement for training data spanning the conditions of interest, which structures in service rarely provide since the damaged states one wishes to detect are precisely those that have not yet occurred.

The Measured Displacement Histories as a Choice

Vibration-based assessments have historically used accelerations. Accelerometers are robust, require no fixed reference, and are readily deployed. Nagayama and Spencer (2007), developing smart sensor networks for this purpose, make the resulting cost structure explicit: the expense of dense monitoring lies in installation, cabling, and power rather than in any individual transducer, and eliminating the cabling is what makes dense arrays economically practical. Their work also identifies the constraints that persist once cables are removed, including finite battery life and the difficulty of synchronizing distributed measurements. Kordestani et al. (2023) construct a normalized energy damage index from trend lines extracted from acceleration records and locate damage in a five-story laboratory building tested on a shaking table and in a numerical arch-tied bridge. Al Jailawi (2020), using angular velocity measured by a gyroscope, reports that the angular-velocity formulation outperformed the acceleration-based approach on the structures examined, showed lower sensitivity to environmental acoustic noise, and remained effective on curved beams where the acceleration-based approach performed poorly. That study also adopts an output-only formulation requiring no knowledge of the input excitation and applies transmissibility and coherence of the measured response to assess the condition of supports resembling bridge bearings.

Displacement occupies a particular position in this discussion. Damage indices of the modal indicator family are formulated in terms of displacement or its spatial derivatives, so displacement is the quantity the indices require. Recovering it from acceleration requires double integration, which amplifies low-frequency noise and introduces drift that must subsequently be removed. Measuring displacement directly avoids that step. The obstacle has historically been practical because contact displacement transducers require a fixed external reference, which is seldom available on a bridge.

Vision-Based Displacement Measurement

Computer vision removes that obstacle. Narazaki et al. (2020) develop dense three-dimensional displacement measurement from video using physics-based graphics models and demonstrate the approach on a laboratory truss. The measurement is non-contact and yields many spatially distributed points from a single instrument. This last property is the significant one for inverse identification, because it addresses directly the imbalance between the number of unknowns and the number of measurements described above. However, optical tracking is subject to image noise and variation in ambient lighting that alters contrast over the duration of a record. Field of view constrains which portion of a structure can be observed, and the recoverable components of motion depend on camera placement.

Environmental conditions affect the response of bridges independently of their condition, and their treatment remains an active research area. Zhu et al. (2023), in a full-scale computational study of wind conditions at the Queensferry Crossing, illustrate the complexity of characterizing such effects on a long-span structure. For laboratory work of the kind reported here, these effects are absent by construction, which is a limitation rather than an advantage, and is identified as such in the conclusion.

Method Selection

The framework adopted in this project combines vision-based displacement measurement with a modal indicator formulation. The selection follows from the constraints identified above.

Model updating was set aside because it requires a validated model of the specific structure under assessment, which is unavailable for most assets an agency must screen, and because the parameter-to-measurement ratio on a member-level assessment makes the updated solution non-unique without strong prior constraints. Data-driven methods were set aside because they require labeled examples of the damage states to be detected, which in-service structures do not supply. Modal indicator methods require only a reference measurement and a test measurement of the same structure, and the reference may be established at any earlier time at which the structure was believed sound. Every subsequent survey is compared against that same fixed reference, so each result is independent and measurement errors do not accumulate across the sequence. This is compatible with how agencies actually manage assets.

Within that family, modal strain energy (MSE) was selected as the primary indicator because the deterioration mechanism of interest is section loss (linear damage such as corrosion) at the member scale. A member losing cross-sectional area softens; its share of the modal strain energy redistributes, and the change is expressed at the element. The known limitation of the family is that indicator magnitude does not map to a physical severity without calibration. That limitation is not avoided in this work; it is quantified in the results and addressed explicitly in the future work.

Vision-based displacement measurement was selected as the input because it supplies the many spatially distributed measurement points the indicator formulation requires, expressed in the physical quantity in which that formulation is written, without integration and without instrumentation attached to the structure. The intent is not to displace contact sensing. A small number of accelerometers remain an effective and affordable means of establishing reference measurements, and the two approaches are complementary; however, reference accelerometers were not used in this project.

Data Description

Small-Scale Warren Truss Specimen

A small-scale Warren truss was used to establish the measurement and identification chain in its simplest form. The truss spans 23 cm between supports and is mounted at its four corners on helical compression springs through spherical magnetic ball joints, with a total assembly mass of 0.323 kg. Because the truss is stiff relative to the springs, the response is dominated by a single fundamental mode, and the system behaves as an equivalent single-degree-of-freedom oscillator. This configuration was chosen deliberately: it reduces the identification problem to a single parameter and therefore allows the video measurement and the parameter extraction to be assessed without the confounding effects of multiple closely spaced modes.

Free vibration records of nine seconds were acquired for a reference state and for a modified state in which the support stiffness was reduced. Damage in this specimen is therefore global, and the quantity identified is the equivalent lateral stiffness of the assembly.

Fourteen-Bay Benchmark Truss Specimen

Element-level work used the fourteen-bay spatial truss benchmark of Narazaki et al. (2020). The specimen is constructed from steel hollow circular members of uniform section with rigid connections at all panel points. Each bay is 0.40 m long and 0.40 m high, giving an overall span of 5.6 m. Damage is introduced by physically reducing the cross-section of selected members, and the prescribed reductions are documented for the specimen, which provides quantified member-level ground truth of a kind rarely available outside the laboratory. Figure 1 shows the benchmark truss configuration. The photograph of the physical specimen is reproduced from Narazaki et al. (2020); the numerical model was developed for this project.

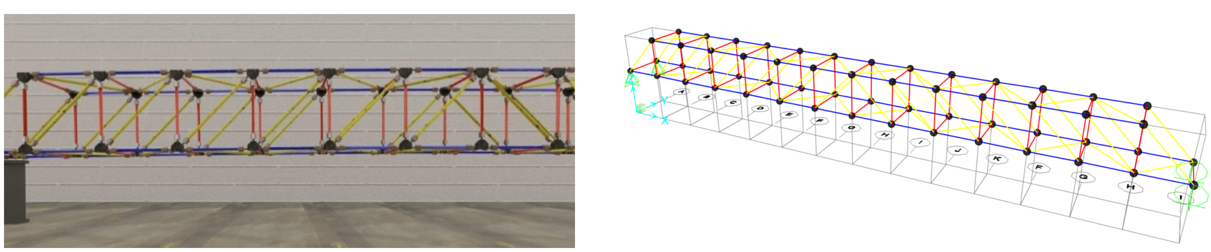

Physical specimens (Narazaki et al. 2020). Numerical Model

Figure 1. Benchmark truss

A finite-element model of the specimen was developed with 56 nodes, mirroring the geometry and the joint idealization. The model was tuned to the first two reference modes of the physical truss, the first transverse bending mode near 21.6 Hz and the first vertical bending mode near 26.4 Hz, so that the simulated response resembles the measured behavior. Section loss is represented in the model by parametric reduction of cross-sectional area.

Damage Cases

Two damage cases are reported from the physical specimen. The first, designated Damage 1, is a lower-chord member, Element 12, with a documented section reduction of 52.7 %. The second, designated Damage 6, is a vertical member, Element 23, with a documented reduction of 88.0 %. These two were selected because they represent different member families and different severities, and because the contrast between them exposes the influence of the measurement configuration on localization performance.

The finite-element study covers a wider range. Three representative members were examined, one diagonal, one lower chord, and one vertical, each at prescribed stiffness reductions from 10 to 90 %. This range was used to characterize how localization performance and indicator magnitude vary with severity under conditions in which the ground truth is exact and the measurement is free of optical error.

Measurement Configuration

Displacement was extracted from single-camera video of the benchmark truss. Field-of-view constraints limited the measurement to the portion of the span visible to the camera, within which sixteen panel points were tracked: eight on the lower chord and eight on the upper chord. Figure 2 identifies these points as they appear in the camera view, numbered from left to right, with points 0 through 7 on the lower chord and points 8 through 15 on the upper chord.

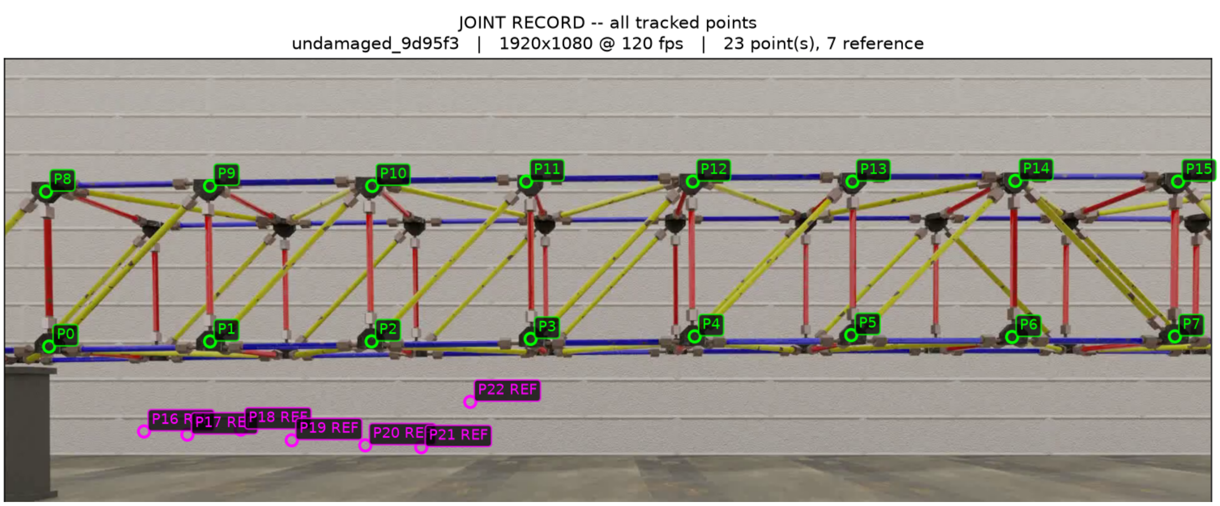

Figure 2. Tracked points on the benchmark truss, numbered left to right (green tracked structural points, magenta points are reference).

Measurements were recorded in the vertical direction only, at a sampling rate of 250 Hz. The measured configuration therefore comprises sixteen single-degree-of-freedom channels. The finite-element study, by contrast, provides 112 channels, corresponding to 56 joints with two in-plane degrees of freedom each. The measured case represents a sevenfold reduction in degrees of freedom relative to simulation, with the horizontal direction unmeasured. This constraint is the principal limitation on element-level resolution in the measured results and is referred to throughout the discussion that follows. The horizontal component is recoverable from the same video; it was excluded because documented ground truth was available only for the vertical direction, so results from the horizontal direction could not have been validated against a known reference.

Methodology

This section sets out the processing chain from recorded video to element-level damage indicator. The chain has four stages: extraction of displacement from video, output-only identification of modal parameters, quantification of the uncertainty in those parameters, and formation of the damage index. Each stage is described in the order applied, and every symbol is defined in the text immediately following the equation in which it first appears.

Displacement Extraction from Video

Displacement is extracted using the Lucas-Kanade optical flow algorithm with pyramidal refinement. The algorithm assumes that the image intensity of a moving feature is conserved between consecutive frames and that motion is locally uniform within a small neighborhood surrounding the tracked point. Under these assumptions, the displacement increment between frames is the vector that minimizes the summed squared intensity difference over the neighborhood,

$$d_k = arg\, min\, \Sigma_{x \in W} \, [I(x, t_k) - I(x + d, t_{k+1})]^2 \tag{1}$$

where d_k is the displacement increment of the tracked point between frames k and $k+1$, expressed in pixels; $I(x, t)$ is the image intensity at pixel coordinate x and time t; x is a pixel coordinate lying within the tracking window W, which is the neighborhood over which motion is assumed to be uniform; t_k is the time of frame k; and d is the trial displacement vector over which the minimization is performed.

The pyramidal extension performs this minimization at successively finer image scales, so that displacements larger than the window can be recovered from the coarse levels and refined at the fine levels. This improves robustness to large motion, to lighting variation, and to motion blur.

Pixel motion is converted to metric units through a scale factor determined from a known reference dimension visible in the field of view,

$$u(t) = \lambda \cdot p(t), \quad \lambda = \frac{L}{L_{pix}} \tag{2}$$

in which $u(t)$ is the physical displacement of the tracked point, in meters; $p(t)$ is the motion of that point measured in the image, in pixels; λ is the scale factor converting image motion to physical displacement, in meters per pixel; L is a reference length measured on the structure itself, in meters; and L_{pix} is the extent of that same reference length as it appears in the image, in pixels.

Each extracted channel was conditioned before identification by outlier rejection, median filtering, removal of drift by high-pass filtering at 0.2 Hz, and band-limiting at 40 Hz.

Output-Only Modal Identification

Modal parameters are identified without knowledge of excitation, which is necessary because the excitation acting on an operating structure is not measurable in general. Candidate resonant frequencies are first screened from Welch power spectral density estimates of the individual channels. Natural frequencies, damping ratios, and mode shapes are then obtained by Enhanced Frequency Domain Decomposition (EFDD), in which the matrix of cross-spectral densities between all measured channels is decomposed at each frequency line by singular value decomposition,

$$G_{yy}(j\omega) \ = \ U(j\omega)\, S(j\omega)\, U(j\omega)^H \tag{3}$$

where $G_{yy}(j\omega)$ is the cross-spectral density matrix of the measured channels evaluated at circular frequency ω, in radians per second; $U(j\omega)$ is the matrix whose columns are the left singular vectors; $S(j\omega)$ is the diagonal matrix of singular values, ordered largest first; and the superscript H denotes the Hermitian, that is the complex conjugate, transpose.

At a frequency line dominated by a single mode, the first singular value is much larger than the remainder, and the corresponding first singular vector approximates the mode shape. Damping is estimated from the shape of the first singular value in the neighborhood of the peak.

Modes must be paired between the reference and test states before any comparison is made, because the damage index compares the behavior of each element between two states, and a comparison drawn between mismatched modes produces a result that resembles damage. Pairing uses proximity in frequency together with similarity in shape, the latter assessed by the Modal Assurance Criterion (MAC),

$$MAC(\varphi^H, \varphi^D) \ = \ \frac{|\varphi^{H^{\mathrm{T}}} \varphi^D|^2}{(\varphi^{H^{\mathrm{T}}} \varphi^H)(\varphi^{D^{\mathrm{T}}} \varphi^D)} \tag{4}$$

where MAC is a scalar lying between zero and one; φ^H is the mode shape vector identified in the healthy reference state; φ^D is the corresponding vector identified in the damaged test state; and the superscript T denotes the vector transpose.

The criterion returns unity when the two vectors describe the same deformation pattern and approaches zero when they are orthogonal. Pairs were accepted at a threshold of 0.80.

Uncertainty Quantification

The identification is repeated under bootstrap resampling of the multichannel records. Each realization is formed by resampling with replacement and adding a perturbation of one percent of the record amplitude. Repeating the full identification on every realization yields a distribution for each identified quantity, from which the coefficient of variation is formed,

$$CV(\theta) \ = \ \frac{\sqrt{\frac{\sum_{b=1}^{B} (\theta_b - \theta)^2}{B-1}}}{\theta} \tag{5}$$

where $CV(\theta)$ is the coefficient of variation of the identified quantity θ, which may be a natural frequency, a damping ratio, or a component of a mode shape; θ_b is the value of that quantity obtained in bootstrap realization b; $\bar{\theta}$ is its mean across all realizations; and B is the number of realizations, of which twenty were used.

The dispersion obtained in this way informs the tolerances applied when pairing modes, so that acceptance of a pair reflects the precision achieved.

Elemental Modal Strain Energy

The damage index used in this work is the elemental modal strain energy change, denoted EMSE. It follows the modal strain energy change approach of Shi et al. (2000), but is formed as the relative change in the modal strain energy of each element between states rather than as the strain energy change ratio defined in that work. The computation proceeds through Equations 6 to 10.

For each paired mode and each element, the relative motion of the two end nodes is projected onto the element axis to obtain an axial deformation,

$$\Delta u_{e,m} = \left(\varphi_{j,m} - \varphi_{i,m}\right) \cdot n_e \tag{6}$$

where $\Delta u_{e,m}$ is the axial deformation of element e in mode m, the index e running over the elements of the structure and the index m over the modes successfully paired between states; i and j denote the two end nodes of element e; $\varphi_{i,m}$ and $\varphi_{j,m}$ are the mode shape vectors at those nodes in mode m; and n_e is the unit vector directed along the axis of the element.

Equation 6 requires both in-plane components of the mode shape at each end node. In the finite-element study, both components are available, and the projection is formed directly. In the video study, only the vertical component was measured, so the projection cannot be evaluated, and the relative vertical displacement is used in its place,

$$\Delta u_{e,m} \approx |\, \varphi_{j,m}^{Z} - \varphi_{i,m}^{Z} \,| \tag{7}$$

in which $\varphi_{i,m}{}^{z}$ and $\varphi_{j,m}{}^{z}$ are the vertical components of the mode shape at nodes i and j, respectively, in mode m.

This substitution is exact for members whose axis is vertical, partial for diagonals, and orthogonal to the member axis for chord members. Its consequences for localization are examined in the results.

The modal strain energy stored in an axially deforming member is

$$SE_{e,m} = \frac{1}{2} k_e \left(\Delta u_{e,m}\right)^2, \quad k_e = \frac{E_e A_e}{L_e} \tag{8}$$

where $SE_{e,m}$ is the modal strain energy of element e in mode m; k_e is the axial stiffness of that element; E_e is its elastic modulus; A_e is its cross-sectional area; and L_e is its length.

Element stiffness is not identifiable from output-only displacement measurement, since neither the modulus nor the section is recovered by the identification. The squared axial deformation is therefore adopted as a strain energy proxy, and the axial stiffness is treated as constant between the two states so that it cancels out the relative change formed in Equation 10. This is the reason the index localizes damage but does not by itself measure its magnitude, and it is the origin of the calibration requirement discussed in the results.

Contributions are aggregated over the paired modes by unweighted averaging,

$$SE_e = \frac{1}{M}\sum_{m=1}^{M} SE_{e,m} \tag{9}$$

where SE_e is the modal strain energy of element e aggregated over the paired modes, and M is the number of modes successfully paired between the healthy and damaged states.

The index is then formed as the magnitude of the relative change in that aggregated energy between the two states,

$$EMSE_e = \frac{|\, SE_e^D - SE_e^H \,|}{SE_e^H} \tag{10}$$

where $EMSE_e$ is the elemental modal strain energy change index for element e; SE_e^H is the aggregated modal strain energy of that element in the healthy reference state; and SE_e^D is the corresponding quantity in the damaged test state.

A small-energy guard prevents division by a near-zero baseline. In the finite-element analysis, elements whose healthy energy falls below a threshold of ten to the power minus six times the maximum are masked and assigned a zero index. In the video analysis, the denominator is clamped at machine precision. Elements lying near the guard threshold are interpreted with corresponding caution.

Normalization and Interpretation of the Indicator

For ranking and display, the index is normalized across all evaluable members and expressed on a scale from zero to one hundred,

$$Score_e = 100 \cdot \frac{EMSE_e}{max_f\ EMSE_f} \tag{11}$$

where $Score_e$ is the normalized indicator score for element e, on a scale from zero to one hundred, and the maximum appearing in the denominator is taken over the index f, which runs across all evaluable elements of the structure.

Equation 11 is monotone in the underlying index, so the ranking it produces is preserved, and comparison between members remains meaningful. Two properties of the mapping govern how its output must be read. It assigns exactly one hundred to the highest-ranked element in every analysis, independent of the actual severity, so the value attached to the top-ranked member conveys rank rather than magnitude. It is also uncalibrated, in that no scaling has been fitted against known section loss. The reported score is therefore a normalized indicator magnitude and a ranking device, not a stiffness-loss estimate, and it is used as such throughout the results.

Global Identification for the Single-Degree-of-Freedom Case

For the spring-mounted prototype, for which the response is dominated by a single mode, the identification reduces to three scalar quantities obtained directly from the free vibration record. Damping is determined by a logarithmic decrement, formed from the ratio of two peak amplitudes separated by a whole number of cycles,

$$\delta = \frac{1}{n} \ln \frac{u_i}{u_{i+n}} \tag{12}$$

where δ is the logarithmic decrement; u_i is the amplitude of the *i-th* peak in the decaying response; u_{i+n} is the amplitude of the peak occurring n cycles later; and n is the number of cycles separating the two peaks.

from which the damping ratio follows,

$$\zeta = \frac{\delta}{\sqrt{4\pi^2 + \delta^2}} \tag{13}$$

in which ζ is the damping ratio, expressed as a fraction of critical damping.

The equivalent stiffness is recovered inversely from the identified natural frequency and the known assembly mass,

$$k = \omega_n{}^2\, m = (2\pi f_n)^2\, m \tag{14}$$

where k is the identified equivalent stiffness of the assembly; ω_n is the identified circular natural frequency, in radians per second; f_n is the same frequency expressed in hertz; and m is the equivalent mass of the oscillating assembly. And the global damage index is the relative reduction in stiffness measured against a reference state,

$$D = \frac{k_0 - k}{k_0} \tag{15}$$

where D is the global damage index, and k_0 is the equivalent stiffness identified in the reference state, when the assembly was believed sound. Writing $\Delta k = k_0 - k$ for the stiffness lost between the two states, the index is equivalently $D = \Delta k/k_0$, the form used in Table 1: it expresses how much of the original stiffness has been lost, as a fraction of the sound-state value

Equation 14 requires the equivalent mass to be known independently. In the prototype, this condition is satisfied because the assembly mass was measured directly. On a structure for which the mass is uncertain, Equation 14 yields the ratio of stiffness to mass rather than the stiffness itself, and Equation 15 remains valid only to the extent that the mass is unchanged between the two states.

Results

Global Damage Identification from a Single Tracked Joint

The first study establishes that structural diagnostics can be obtained from video tracking of one point. A single joint on the spring-mounted Warren truss was tracked through a nine-second free vibration record. Damping was determined by the logarithmic decrement method from the ratio of successive peak amplitudes. The natural frequency was identified from the small-amplitude portion of the decay, where the response is closest to linear, and the equivalent stiffness (k) was recovered inversely from Equation 14 using the known assembly mass.

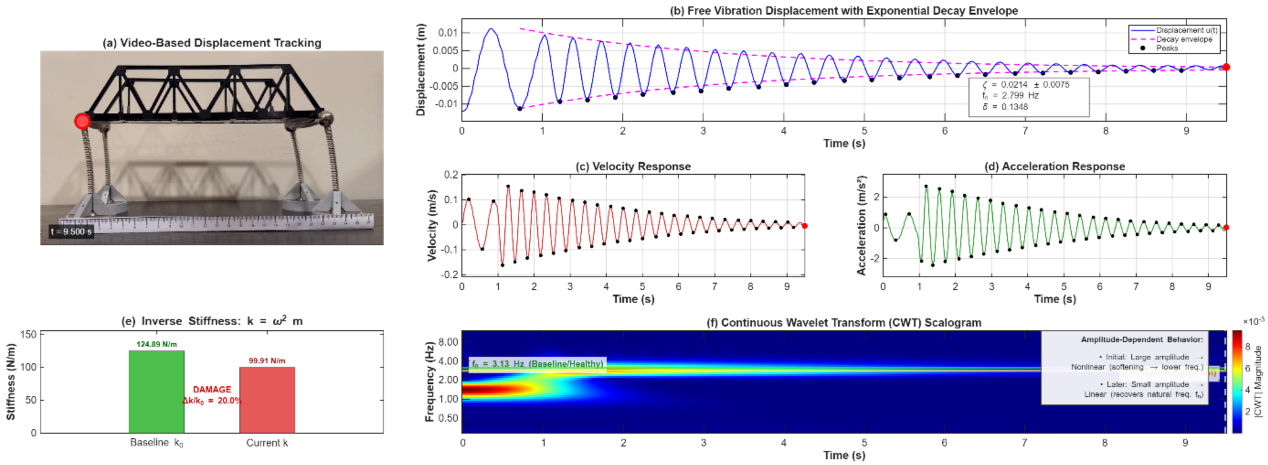

Figure 3. Integrated identification from single-point video tracking.

Table 1 summarizes the identified parameters. The identified frequency of 2.799 Hz with an equivalent mass of 0.323 kg yields a current stiffness of 99.91 N/m, against a reference value of 124.89 N/m established from an earlier test in the sound state. The resulting damage index is a stiffness reduction of 20.0 %.

Table 1. Identified parameters from single-point video tracking.

Parameter	**Identified Value**
Logarithmic decrement δ	0.1348
Damping ratio ζ	0.0214 ± 0.0075 (2.14%)
Natural frequency ω_n	17.586 rad/s
Natural frequency f_n	2.799 Hz
Equivalent mass m	0.323 kg
Reference stiffness k_0	124.89 N/m
Current stiffness k	99.91 N/m
Damage index $\Delta k/k_0$	**20.0%**

The continuous wavelet transform of the record shows two frequency regimes: a lower frequency during the first two seconds, when amplitudes are large, and the spring supports behave nonlinearly, rising asymptotically to the stable linear natural frequency as the oscillation decays. Identifying the frequency from the small-amplitude regime is necessary.

This study establishes the measurement chain but not localization. A single tracked point answers whether the structure has changed; it cannot indicate where. That limitation motivates the multi-point work reported below.

Element-Level Localization from Simulated Response

The second study establishes localization under controlled conditions. Finite-element response of the benchmark truss was computed for the healthy state and for each prescribed damage case, contaminated with synthetic noise, and processed through the identical identification and indexing chain used for measured data. Because the ground truth is exact and the measurement is free of optical error, this study isolates the behavior of the method itself.

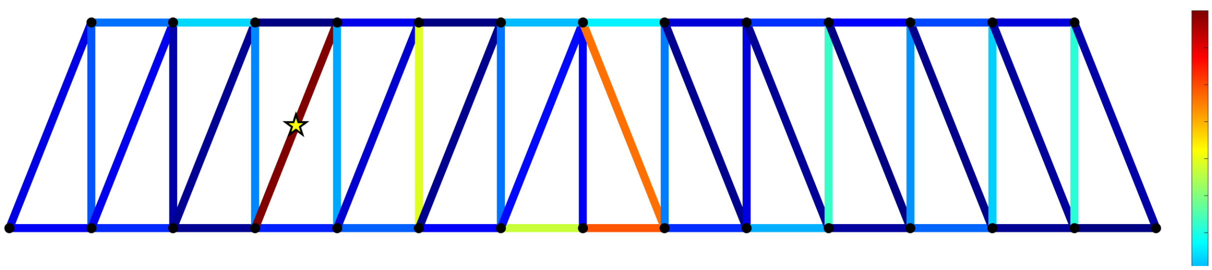

Figure 4. EMSE indicator map, diagonal member with 50 % section loss.

At 50 % section loss, the damaged member is ranked first in all three families examined, and indicator activity is confined to the correct bay. Secondary activity appears on members that share a load path with the damaged element, which is physically interpretable. Table 2 summarizes performance across severities.

Table 2. Localization performance by element family and severity, simulated response.

Family	10-20% loss	30-50% loss	60% loss and above
Lower chord	Truth within top three; activity stays on the lower chord in the truth bay ±1	Truth ranked first; neighbors follow with lower scores	Stable and chord-confined; negligible upper or vertical activation
Vertical	Bay-correct co-activation with the same-panel upper chord; truth often ranked second	Dominant vertical and same-panel pair; diagonals and chords do not intrude	Same pair remains dominant with stronger contrast
Diagonal	Truth diagonal distinctive; support on same-panel chords	Truth diagonal consistently ranked first; support remains bay-confined	Highest contrast, still bay-confined

Two findings follow. Element-level identification is reliable from about 30 % section loss upward. Below that, the true member is not consistently ranked first, but indicator activity nonetheless remains within the correct bay. The bay, rather than the individual member, is therefore the reliable reporting unit at low severity.

Severity Calibration and Family-Specific Behavior

Comparing the normalized indicator score against the prescribed reduction reveals systematic, family-dependent behavior. The relationship is monotone in every family, so ranking and screening decisions are sound. It is not, however, a one-to-one relationship, and the departure differs by family.

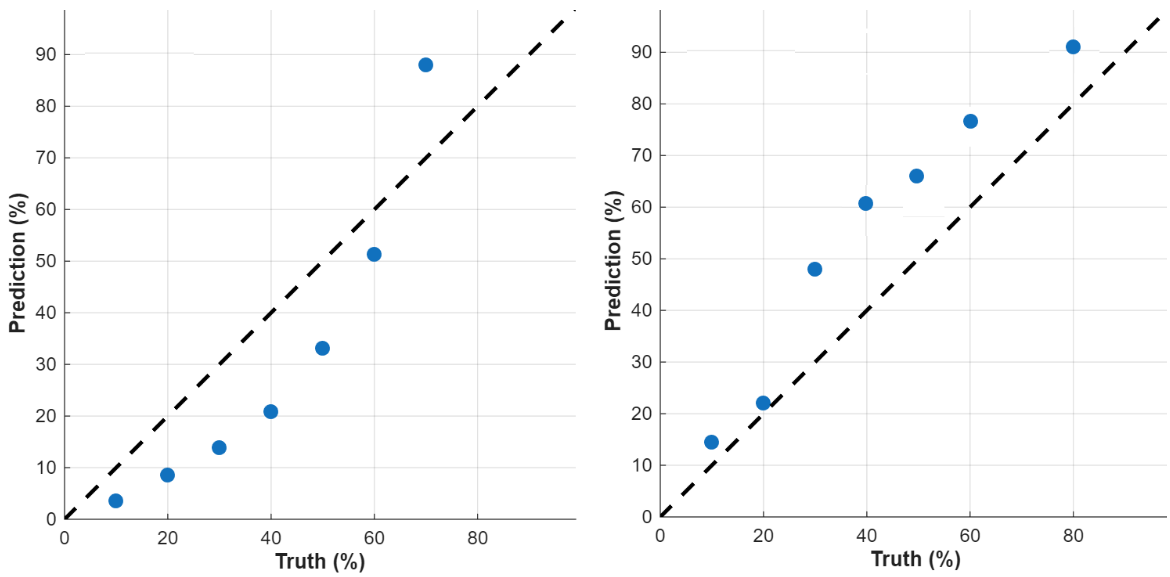

Figure 5. Indicator score against prescribed section loss: damaged diagonal (left) and damaged lower chord (right).

The diagonal case preserves rank ordering but under-predicts through the mid-range and rises steeply at the highest severities, giving a concave characteristic. The lower-chord case is close to linear but lies consistently above the one-to-one line, indicating a family-wide positive bias.

This behavior has a direct explanation in the formulation. The normalization applies a single global scaling to every element, but different families produce systematically different raw indicator magnitudes for the same physical section loss, because their strain-energy participation differs by geometry and load path. One global constant cannot fit all three families simultaneously, and the family-specific departures seen in Figure 5 are the consequence. The remedy is to fit the scaling separately for each family against known ground truth, which the controlled cases reported here would support. Until that calibration is performed, the indicator is adequate for ranking and screening but should not be reported as quantitative severity.

Element-Level Localization from Video-Derived Displacement

The third study applies the identical methodology to displacement extracted from video of the physical specimen. The truss configuration and the damage cases are unchanged; only the data source differs. These records carry sources of uncertainty absent from simulation, including feature misidentification, image noise, and variation in ambient lighting that alters contrast and marker visibility over the duration of a record. They are correspondingly more representative of field conditions and more difficult to interpret.

Results are reported as the rank of the true element and the spatial pattern of indicator activity. The numeric values annotated in the maps are normalized indicator scores, not stiffness-loss estimates, and are interpreted according to the properties of the mapping set out in the methodology.

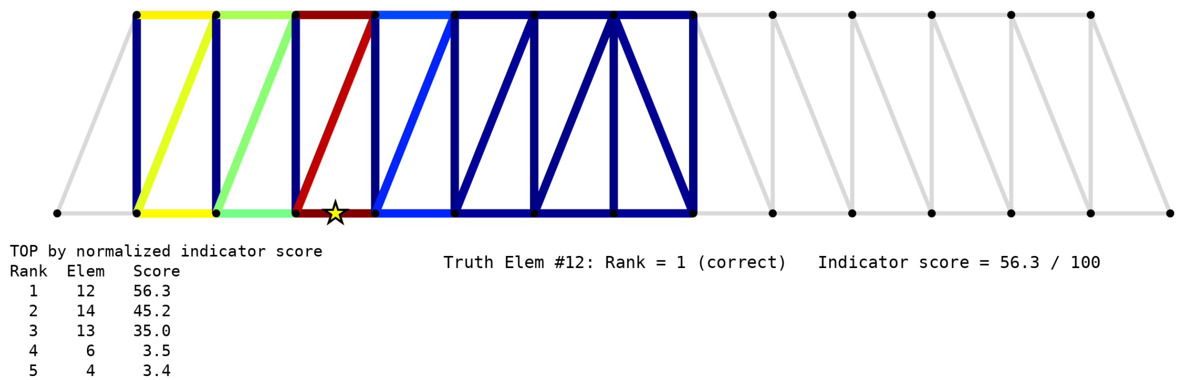

Figure 6. Damage indicator map, Damage 1 (Element 12, lower chord, 52.7 % documented section loss).

For the lower-chord case, the true element is ranked first. Confidence is nonetheless distributed along the lower chord, with Elements 14 and 13 following at appreciable magnitude before a sharp drop to the remaining members, forming a halo confined to the truth bay and its immediate neighbors.

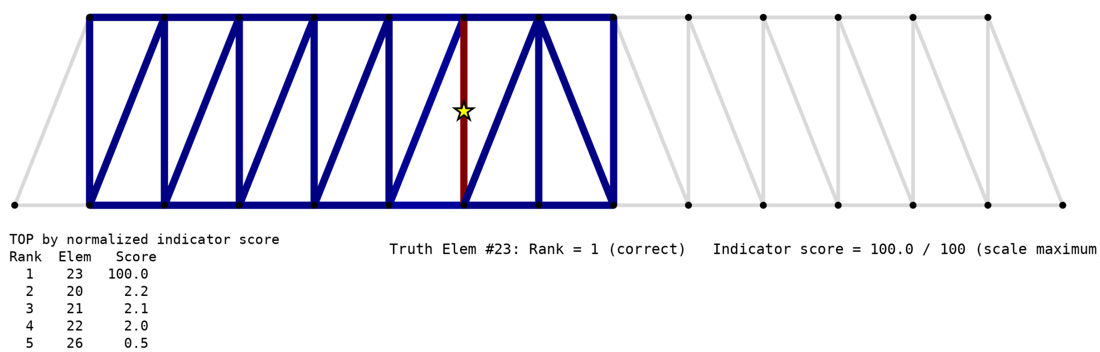

Figure 7. Damage indicator map, Damage 6 (Element 23, vertical, 88.0 % documented section loss).

For the vertical case, the true element is likewise ranked first, and the result is sharply isolated: the next-ranked members fall below 2.2 on the normalized scale, and the hotspot is confined to a single panel.

Interpretation of the Contrast Between Cases

The difference between the two cases is not incidental; it follows from the measurement configuration. Because only the vertical component was measured, the relative end-node motion used in the index is the vertical difference rather than the true axial deformation. For a vertical member, the two end nodes lie on opposite chords, and their vertical difference is precisely the member's axial stretch, so the index recovers the intended quantity and the response is sharp. For a lower-chord member, both end nodes lie on the same chord and move almost identically in the vertical direction when the truss deflects as a beam, so the index sees little contrast between the damaged member and its neighbors, and the response spreads along the chord.

The halo in the lower-chord case is therefore a predictable consequence of measuring one component rather than a deficiency of the index. The horizontal component is recoverable from the same recordings, and resolving the axial deformation of chord and diagonal members would require only that it be included in the index. It was not used here because the benchmark specimen provides documented section reductions against which only the vertical channel could be validated. Recovering and validating the horizontal component is expected to sharpen chord and diagonal localization specifically.

Taken together, the video results demonstrate that the framework tolerates realistic measurement uncertainty. Both cases achieved rank-one identification of the damaged member within the correct bay, using sixteen channels in a single direction, from a single camera, with no instrumentation attached to the structure.

Conclusion

Findings

This project developed and validated an inverse problem framework for bridge structural health monitoring using displacement as the primary diagnostic input and demonstrated it on truss specimens through three progressive laboratory studies.

Video tracking of a single joint on the spring-mounted Warren truss recovered damping, natural frequency, and equivalent stiffness, and identified a 20.0% stiffness reduction against a reference state. This establishes that the measurement and identification chain functions end to end, while confirming that a single tracked point can detect change but cannot locate it.

Applied to the fourteen-bay benchmark truss with simulated response, the elemental modal strain energy index localized damage at the element level in all three member families at 50% section loss, with activity confined to the correct bay and secondary response following interpretable load paths. Localization is reliable from approximately 30 % loss upward; below that threshold the true member is not consistently ranked first, although activity remains bay-confined.

Applied to video-derived displacement from the same specimen, the framework identified the damaged member at rank one in both cases examined, using sixteen channels in the vertical direction only. The vertical member produced a sharply isolated response and the lower-chord member a halo along the chord, a contrast that follows directly from measuring a single displacement component.

Limitations

Two limitations bound these findings. The severity mapping is uncalibrated: it assigns the maximum of its scale to the highest-ranked element by construction and applies one global scaling to families that respond differently, so reported scores support ranking but not quantitative severity. The second is that the work was conducted entirely on laboratory specimens under controlled conditions, so the environmental and operational variability that affects structures in service, including temperature, humidity, ambient lighting, and traffic loading, has not been assessed.

The scope of the demonstration is also bounded by structural type. Both specimens are trusses, and the damage index used here assumes deterioration by axial section loss in discrete members. Other bridge forms, girder, slab, arch, and cable-supported structures, deteriorate by mechanisms that this index does not represent, and would require damage indicators formulated for those mechanisms. The framework is therefore demonstrated for truss structures; extension to other forms is a matter of selecting an appropriate indicator, not of re-deriving the measurement and identification chain.

Future Work

The priority is calibration of the indicator-to-severity mapping on an element-family basis, fitted against the controlled cases already available, which would convert the present ranking output into a quantitative severity estimate. The second is extension to low-severity damage through bay-level aggregation, since indicator activity remains bay-confined at severities where element-level ranking degrades; a bay-level index is expected to be the reliable reporting unit in the range most relevant to early intervention. Beyond these, field application to an in-service structure is the natural next stage. Discussions with the District Department of Transportation (DDOT) have identified the possibility of applying the framework to a DDOT-owned bridge in Washington, DC. Possible deployment would follow completion of the calibration work described above, since severity estimates on an un-instrumented in-service structure cannot be interpreted until the indicator-to-severity mapping has been calibrated against known ground truth, together with an assessment of the environmental and operational variability absent from the laboratory.

References

Al Jailawi, S. S. H. (2020). "Damage detection using angular velocity." Doctoral dissertation, University of Iowa, Iowa City, IA. https://doi.org/10.17077/etd.ufhp-2zhq

Bao, Y., Sun, H., Xu, Y., Guan, X., Pan, Q., and Liu, D. (2025). "Recent advances in structural health diagnosis: a machine learning perspective." *Advances in Bridge Engineering*, 6, 7.

Catbas, F. N., Brown, D. L., and Aktan, A. E. (2006). “Use of modal flexibility for damage detection and condition assessment: Case studies and demonstrations on large structures.” Journal of Structural Engineering, 132(11), 1699–1712.

Cawley, P., and Adams, R. D. (1979). “The location of defects in structures from measurements of natural frequencies.” Journal of Strain Analysis for Engineering Design, 14(2), 49–57.

Friswell, M. I. (2007). “Damage identification using inverse methods.” Philosophical Transactions of the Royal Society A, 365(1851), 393–410.

Gallet, A., Rigby, S., Tallman, T. N., Kong, X., Hajirasouliha, I., Liew, A., Liu, D., Chen, L., Hauptmann, A., and Smyl, D. (2022). “Structural engineering from an inverse problems perspective.” Proceedings of the Royal Society A, 478(2257), 20210526.

Hester, D., Koo, K., Xu, Y., Brownjohn, J., and Bocian, M. (2019). “Boundary condition focused finite element model updating for bridges.” Engineering Structures, 198, 109514.

Kordestani, H., Zhang, C., and Masri, S. F. (2023). “Normalized energy index-based signal analysis through acceleration trendlines for structural damage detection.” Measurement, 210, 112530.

Nagayama, T., and Spencer, B. F., Jr. (2007). Structural health monitoring using smart sensors. NSEL Report Series No. NSEL-001, University of Illinois at Urbana-Champaign.

Narazaki, Y., Gomez, F., Hoskere, V., Smith, M. D., and Spencer, B. F., Jr. (2020). “Efficient development of vision-based dense three-dimensional displacement measurement algorithms using physics-based graphics models.” Structural Health Monitoring, 20(4), 1841–1863.

Pandey, A. K., Biswas, M., and Samman, M. M. (1991). “Damage detection from changes in curvature mode shapes.” Journal of Sound and Vibration, 145(2), 321–332.

Shi, Z. Y., Law, S. S., and Zhang, L. M. (2000). “Structural damage detection from modal strain energy change.” Journal of Engineering Mechanics, 126(12), 1216–1223.

Zhu, L., McCrum, D., Sweeney, C., and Keenahan, J. (2023). "Full-scale computational fluid dynamics study on wind condition of the long-span Queensferry Crossing Bridge." *Journal of Civil Structural Health Monitoring*, 13, 615–632.